*Stars and their variability observed from space*
*C. Neiner, W. W. Weiss, D. Baade, R. E. Griffin, C. C. Lovekin, A. F. J. Moffat (eds)*

# CHEOPS & STARS (& ASTEROSEISMOLOGY)

S. Barceló Forteza[1], A. Moya[2], A. Bonfanti[3], S.J.A.J. Salmon[3], V. Van Grootel[3] and D. Barrado[1]

**Abstract.** The characterization of exoplanets has been considerably improved during the last decade mainly through space missions (*Kepler/K2*, *CoRoT*) and also the characterization of their host stars by stellar seismology. Nowadays, *TESS* and *CHEOPS* are the only two important missions that will provide short-cadence high-precision photometric time-series for a large amount of targets. This project explored the asteroseismic potential of *CHEOPS* light-curves. For that purpose, we analysed the probability of detecting solar-like pulsations, and the accuracy we could obtain for estimates of the seismic indices for the expected targets, observing time and expected duty cycle of this mission. Our results suggested that we can determine the frequency at maximum power for evolved and/or massive F-G-K solar-like stars with an uncertainty better than 5%. Asteroseismology therefore enables us to decrease age, mass, radius and density uncertainties significantly in the characterization of exoplanet host stars.

Keywords: stars: fundamental parameters, stars: solar-type, asteroseismology

## 1 Introduction

*CHEOPS* (Fortier et al. 2014) will be the next ESA space mission to study transiting exoplanetary systems accurately. Moya et al. (2018) explored the asteroseismic potential of this mission. Asteroseismology enables us to determine the structural parameters of the host stars with higher precision than do other techniques, improving the characterization of the exoplanetary system. For that reason, we estimated the detectability potential of solar-like pulsations in each region of the H–R diagram. In addition, we studied the accuracy we can reach in determining the frequency at maximum power for different observing times and duty cycles. Finally, we analysed the benefits we can derive through accurate seismic analyses with *CHEOPS* light-curves.

## 2 Detectability potential

To estimate the detectability potential of solar-like pulsations, we analysed the probability of a Gaussian-like power excess to differ statistically from noise in the frequency power spectrum. First of all, using semi-empirical relations and stellar models, we estimated the expected strength of stellar pulsations in the power spectrum:

$$P_{tot} = \frac{1}{2} c A_{\max}^2 \eta^2(\nu_{\max}) D^{-2} \frac{W}{\Delta\nu} \text{ ppm}^2, \tag{2.1}$$

where $\Delta\nu$ is the large separation, $\nu_{\max}$ is the frequency at maximum power, $W$ is the pulsational frequency range, and $A_{\max}$ is the expected maximum amplitude of the radial modes ($l = 0$) in parts per million (ppm),

$$A_{\max} = A_{\max,\odot} \beta(T_{\text{eff}}) \left(\frac{R}{R_\odot}\right)^2 \left(\frac{T_{\text{eff}}}{T_{\text{eff},\odot}}\right)^{\frac{1}{2}} \text{ ppm}\,. \tag{2.2}$$

The values of these variables depend on the fundamental parameters of the models such as radius ($R$) and temperature of the star ($T_{\text{eff}}$). The factor c measures the mean number of modes per $\Delta\nu$ segment and depends on the observed wavelength. Since the *CHEOPS* bandpass is similar to that of *Kepler* (see Fig.1 and Gaidos et al. 2017), we have used $c \sim 3.1$ (Chaplin et al. 2011). The attenuation factor, $\eta^2(\nu)$, takes into account the non-zero integration time that affects the measurement of the signal. The dilution factor $D \sim 1$ for an isolated object. In this study we focussed on this isolated star case.

[1] Dpto. Astrofísica, Centro de Astrobiología (CSIC-INTA), ESAC campus, Camino Bajo del Castillo s/n, 28692, Villanueva de la Cañada, Spain.

[2] Electrical Engineering, Electronics, Automation and Applied Physics Department, E.T.S.I.D.I, Polytechnic University of Madrid (UPM), Madrid 28012, Spain

[3] Space sciences, Technologies and Astrophysics Research (STAR) Institute, Université de Liège, Allée du Six Août 19C, B-4000, Liège, Belgium.

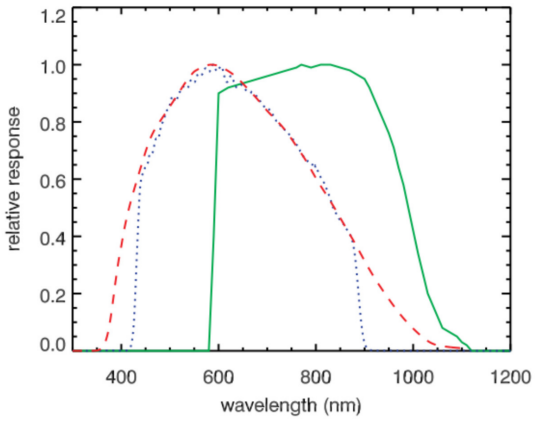


**Fig. 1.** The predicted or established response functions of *TESS* (solid green), *Kepler* (dotted blue), and *CHEOPS* (dashed red), all normalized to unit maximum. See Gaidos et al. (2017).

Next, we estimated the background power coming from different sources:

$$B_{tot} \approx W\,(b_{instr} + P_{gran})\;ppm^2, \tag{2.3}$$

where $b_{instr}$ is the instrumental noise and $P_{gran}$ the stellar granulation power. The instrumental noise follows the form

$$b_{instr} \approx 2 \times 10^{-6} \sigma \Delta t\, ppm^2 \mu Hz, \tag{2.4}$$

where $\sigma$ is the *CHEOPS* predicted RMS noise per given exposure time ($t_{exp}$) and $\Delta t$ is the integration time. The final RMS noise value mainly depends on the stellar magnitude (*CHEOPS* Red Book, 2013), the exposure time, and the integration time. Since *CHEOPS* adds and downloads images every 60 seconds we worked with only one integration time of 60 sec. Table 1 shows the instrumental RMS for three different stellar magnitudes ($V$ = 6, 9, and 12), with three corresponding exposure times (1, 10, and 60 s, respectively). Those values were our reference values.

**Table 1.** Instrumental noise of *CHEOPS* for $\Delta t \sim 60$s.

| $V$ | $t_{exp}$ (s) | $\sigma$ (ppm) |
|---|---|---|
| 6 | 1 | 44 |
| 9 | 10 | 165 |
| 12 | 60 | 623 |

To calculate the stellar granulation noise we use

$$P_{gran} = \eta^2(\nu_{\max}) D^{-2} \sum_{i=1}^{2} \frac{\frac{2\sqrt{2}}{\pi}\frac{a_i^2}{b_i}}{1 + (\frac{\nu_{\max}}{b_i})^4}\, ppm^2 \mu Hz \tag{2.5}$$

from Kallinger et al. (2014), where all parameters depend on $\nu_{\max}$ in the following way

$$\begin{aligned} a_i &\propto \nu_{\max}^{-0.6}\,, \\ b_i &\propto \nu_{\max}\,. \end{aligned} \tag{2.6}$$

For a detailed explanation of the origin and assumptions of these expressions, we refer to Moya et al. (2018) for *CHEOPS*, Chaplin et al. (2011) for *Kepler* and Campante et al. (2016) for *TESS*.

Because of the dependencies of the signal-to-noise ratio ($S/N = P_{tot}/B_{tot}$), the probability to detect solar-like oscillations depends on the structural parameters ($M$, $R$, $T_{\rm eff}$). But it also depends on the observing time ($T$), since the number of bins with information on the power excess in the frequency domain is $N = W\,T$. In addition, we want to ensure cover of at least one entire period of each expected solar-like pulsation. Therefore,

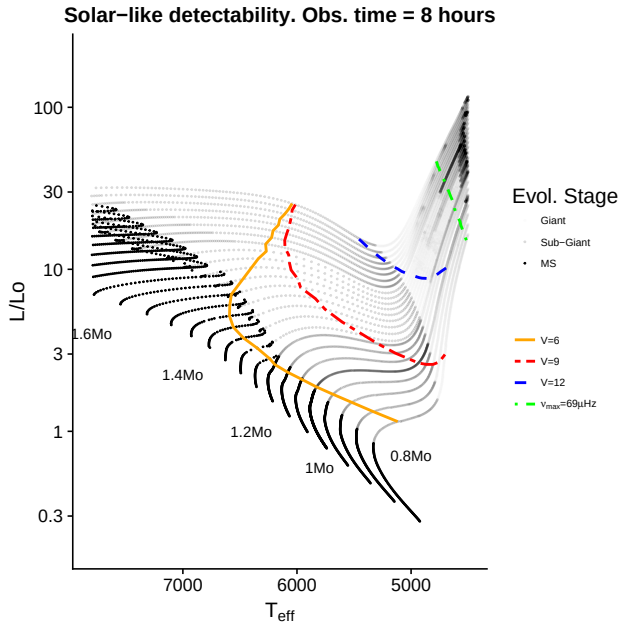


**Fig. 2.** H–R diagram showing the region where $\nu_{\max}$ can be determined, using 8 hours of observing time. Black/dark grey/light grey points are the models of the stars in different evolutionary stages: main-sequence, subgiant and giant stars. The limits of $\nu_{\max}$ detections are represented by orange solid/red dashed/blue dashed-dotted lines for different apparent magnitudes ($V \sim 6, 9, 12$). The green line represents the limit for a correct cover of all pulsations.

another condition to study properly the power excess is $T \geq 2/\nu_{\max}$.

In that way, we calculated for each model the probability of a given excess to differ statistically from noise; Fig. 2 shows the detection limits for $T \sim 8$ hours and our three reference values of stellar magnitude. Each star inside the limited regions has a potentially detectable $\nu_{\max}$. We note that the largest regions of the H–R diagram can be analysed for the brightest stars. In the opposite way, we can make the same study but for fixed stellar magnitude and variable observing times (see Fig. 3). For the longest observing times, the largest regions can then be studied and the longest periods can also be analysed. Fig. 3 also shows (green triangles) the position in the H–R diagram of the 169 exoplanet host-stars located in the ecliptic plane and which can be studied by *CHEOPS*, and weakly covered by *TESS* if so. Each of its panels shows those stars with apparent magnitudes between those presented in the plot (big triangles) and those of the following plot (small triangles).

In summary, *CHEOPS* can potentially obtain the seismic index $\nu_{\max}$ for post- and main -sequence F-G-K stars. Depending on the observing time, tens of stars with planets can be properly characterized.

## 3 Impact of duty cycle on determinations of $\nu_{\max}$

The observing time $T$ has a major impact on the information obtained in the frequency domain. Since the time per target will be of the order of hours or a few days, it is not possible to obtain the parameters of individual modes. Nevertheless, it is sufficient for obtaining the frequency of maximum power. In addition, the duty cycle produces spurious signals that, *a priori*, may affect the determination of this seismic index. We studied the impact of the observing time and duty cycle upon the determination of $\nu_{\max}$.

To study the dependencies of the accuracy upon those parameters, we analysed a group of short-cadence (SC) *Kepler* light-curves of well-studied stars in different evolutionary stages. From those, we could simulate shorter light-curves with lower duty cycles from 60 to 90%. We used CHEOPSim tool in order to obtain the expected duty cycle produced by the South Atlantic Anomaly and Earth occultation. We filled each of the gaps with a linear fit.

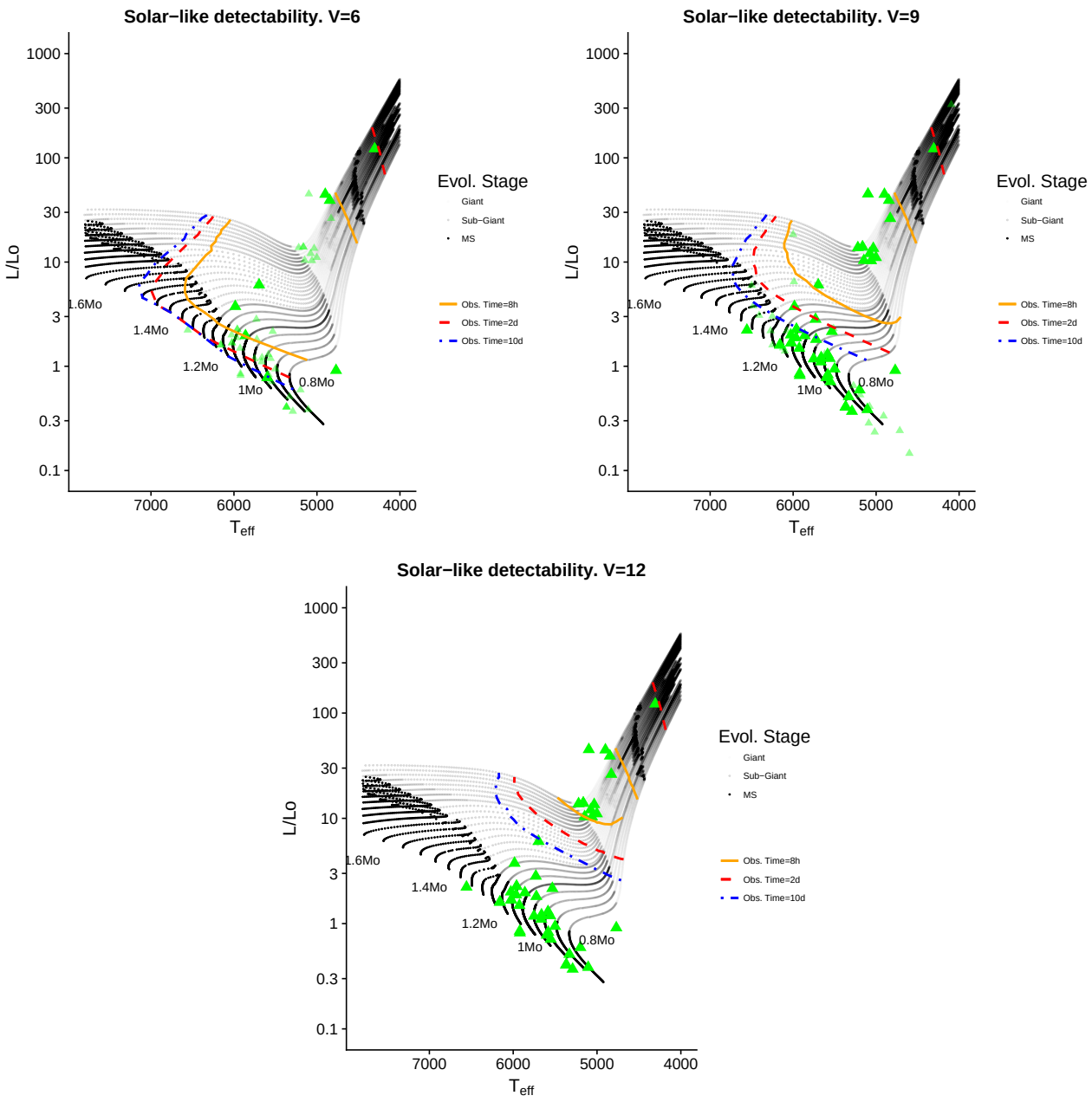


**Fig. 3. Top left panel:** Same as Fig. 2 but with the stellar magnitude fixed at $V \sim 6$, and using different observing times. The limits of $\nu_{\rm max}$ detection are represented by orange solid/red dashed/blue dashed-dotted lines for observing times of 8 hours, 2 days, and 10 days, respectively. Big green triangles indicate the positions of the currently known planet-hosting stars in the ecliptic plane, with $V < 6$. Small and more transparent green triangles are host stars with magnitudes between $6 < V < 9$. **Top right and bottom panel:** Same as top left panel but for stars with $V \sim 9$ and $V \sim 12$, respectively. The big/small green triangles are brighter/fainter than the specified magnitudes.

To calculate $\nu_{\rm max}$, we used the weighted mean frequency (Kallinger et al. 2010):

$$\nu_{\rm max} = \frac{\sum A_i \nu_i}{\sum A_i}\,, \tag{3.1}$$

where $\nu_i$ and $A_i$ are the frequency and the amplitude of each peak of the power excess. We tested the accuracy of the method by comparing the results with the values in the literature for the stars in our sample (e.g. Lund et al. 2017). Fig. 4 shows the relative error of $\nu_{\rm max}$ for three different stars, one per evolutionary stage tested, in 1-day runs with an 80% duty cycle. Although some measurements can have a considerably large relative error,

the mean relative error is appropriate (the red lines in this Figure).

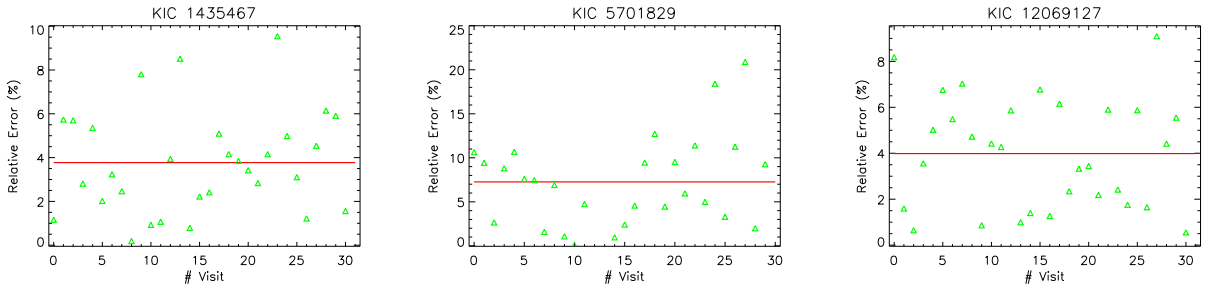


**Fig. 4.** Relative error of $\nu_{\rm max}$ calculated for 1-day runs with an 80% duty cycle. Shown here are the results for a main-sequence star, a subgiant and a red giant, respectively. Each green triangle points to significant detections. The red line represents the mean relative error of $\nu_{\rm max}$ for each star.

Once we had calculated the mean relative error for all stars, we repeated the process for several observing times and duty cycles (see Fig. 5). Our results showed that, in general, the longer the duty cycle and the observing time, the smaller the mean and maximum relative error. The mean relative error ranges from ∼2% for 30-day and 100% duty cycle to ∼4% in the case of 1-day run and 60% duty cycle. The mean maximum error is 11% in this last case. There are no large variations in accuracy for different observing times or duty cycles. However, planning several runs is recommended in order to discard individual measurements that may have large errors. Moreover, it is not worth proposing observing ranges longer than 4 days if several runs are planned. The improvement of maximum and mean relative errors achieved in those cases is non-significant*.

## 4 Benefits of asteroseismology

To characterize a star, we want to obtain its parameters such as effective temperature ($T_{\rm eff}$), metallicity ([Fe/H]), and surface gravity ($\log g$), usually from spectroscopy. Using asteroseismic $\nu_{\rm max}$ with a mean relative error of 5%, we can obtain an independent measure of $\log g$ that is four times more accurate than the spectroscopic value (Moya et al. 2018). Moreover, it is also possible to improve the mean uncertainties of other stellar parameters such as mass (from 2.1% to 1.8%), radius (from 1.8% to 1.6%), density (from 5.6% to 4.7%), and age (from 52% to 38%). These improvements become more significant if we study star-by-star, especially ones beyond the main-sequence turn-off. For example, KIC 5701829 has an age uncertainty of 45% from spectroscopy but only 18% from asteroseismology. Apart from improvements in stellar uncertainties, asteroseismology enables us to remove stellar pulsation signals, so this technique is also useful for improving the accuracy of modelling exoplanet transits.

## 5 Conclusions

Asteroseismology offers us an open window for improving the characterization of some exoplanet(s)-hosting stars and their observed transits. The main advantage is that the seismic analysis can be done with the planned observing strategy and technical characteristics of *CHEOPS*. However, it is only possible for massive and/or post-MS stars. As expected, the longer the observing time, the larger the range of stars that can potentially be characterised with asteroseismology.
The large accuracy achieved for $\nu_{\rm max}$ measurements is sufficient to determine stellar $\log g$ and other stellar characteristics such as age, mass and radius precisely. Unfortunately, this is the only seismic parameter measurable. In any case, it will be helpful for removing the main pulsational signal from the time series.
There are two observational strategies possible: to use comprehensive monitoring of some targets with potentially observable pulsations, and to fill some gaps by monitoring the most interesting targets when not in transit

*We repeated this analysis for $\delta$ Scuti stars instead of solar-like pulsators. The mean relative error was around 5% for observing times down to a few hours and duty cycles higher than 70%. A relative error lower than 10% (5%) was guaranteed for 1-(2-)day light-curves. See Moya et al. (2018) for further details.

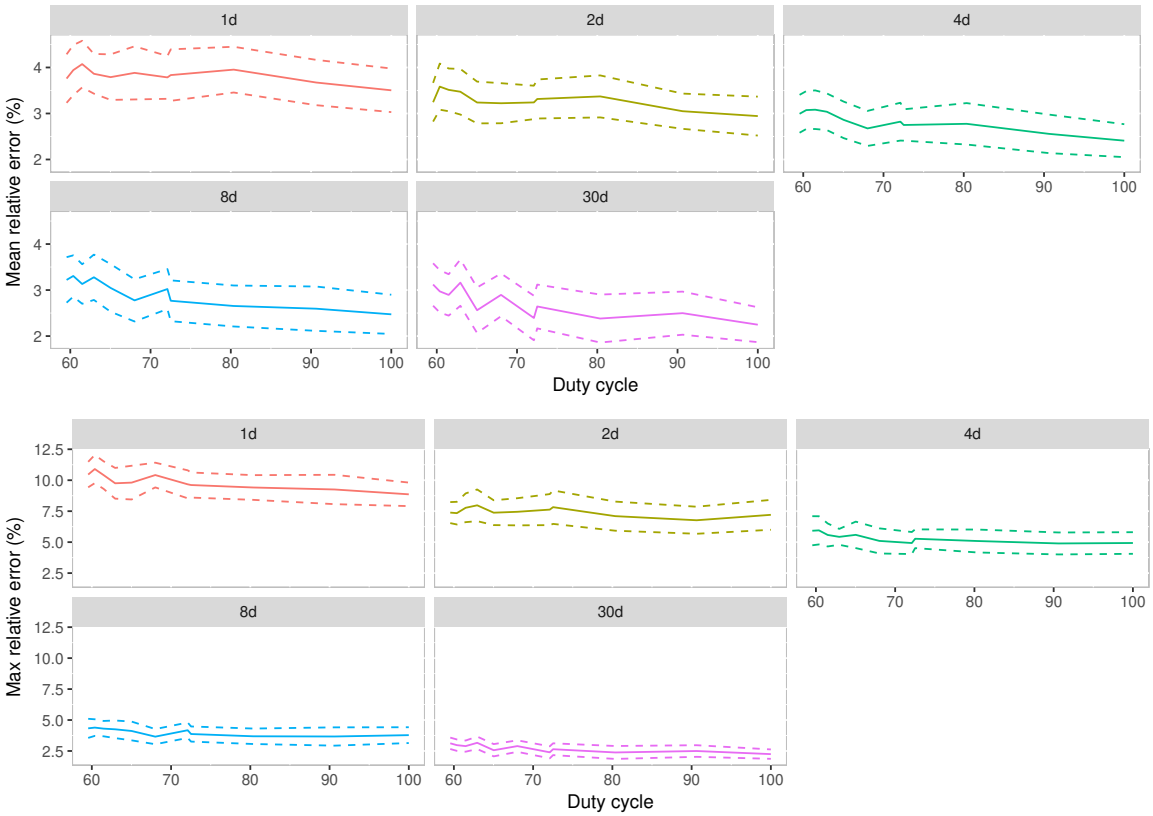


**Fig. 5. Top (Bottom) panels:** Mean (maximum) relative error according to the duty cycle for different observing times. Dashed lines are their standard deviations.

for at least 8 hours.

SBF and DB acknowledge support by the Spanish State Research Agency (AEI) Projects No.ESP2017-87676-C5-1-R and No. MDM-2017-0737 Unidad de Excelencia María de Maeztu- Centro de Astrobiología (INTA-CSIC). AM acknowledges funding from the EU Horizon 2020 research and innovation programme under the Marie Curie grant agreement no. 749962 (project THOT).

## References

Campante, T. L., Schofield, M., Kuszlewicz, J. S., et al. 2016, ApJ, 830, 138
Chaplin, W. J., Kjeldsen, H., Bedding, T. R., et al. 2011, ApJ, 732, 54
Fortier, A., Beck, T., Benz, W., et al. 2014, in SPIE Conference Series, Vol. 9143, Proc. SPIE, 91432J
Gaidos, E., Kitzmann, D., & Heng, K. 2017, MNRAS, 468, 3418
Kallinger, T., De Ridder, J., Hekker, S., et al. 2014, A&A, 570, A41
Kallinger, T., Weiss, W. W., Barban, C., et al. 2010, A&A, 509, A77
Lund, M. N., Silva Aguirre, V., Davies, G. R., et al. 2017, ApJ, 835, 172
Moya, A., Barceló Forteza, S., Bonfanti, A., et al. 2018, A&A, 620, A203